Geologica Acta, Vol.5, Nº 4, 2007, 323-335
Available online at www.geologica-acta.com

geologica acta

Combined use of the GGSFT data base and on board marine collected data to model the Moho beneath the Powell Basin, Antarctica

R.E. CHÁVEZ*[1] E.L. FLORES-MÁRQUEZ[1] E. SURIÑACH[2] J.G. GALINDO-ZALDÍVAR[3] J.R. RODRÍGUEZ-FERNÁNDEZ[4] and A. MALDONADO[4]

[1] **Instituto de Geofísica, UNAM**
Cd. Universitaria, Circuito Exterior, 04510, México, D.F.
Chávez E-mail: exprene@geofisica.unam.mx Flores-Márquez E-mail: leticia@geofisica.unam.mx

[2] **Departament de Geodinàmica i Geofisica, Universitat de Barcelona**
c/ Martí i Franquès, s/n, 08028, Barcelona, España. E-mail: emma.surinach@ub.edu

[3] **Departamento de Geodinámica, Universidad de Granada**
18071 Granada, España. E-mail: jgalindo@ugr.es

[4] **Instituto Andaluz de Ciencias de la Tierra, CSIC-Universidad de Granada**
Facultad de Ciencias, Campus Fuentenueva, s/n, 18002-Granada
Rodriguez-Fernández E-mail: jrodrig@ugr.es Maldonado E-mail: amaldona@ugr.es

*Corresponding author

ABSTRACT

The Powell Basin is a small oceanic basin located at the NE end of the Antarctic Peninsula developed during the Early Miocene and mostly surrounded by the continental crusts of the South Orkney Microcontinent, South Scotia Ridge and Antarctic Peninsula margins. Gravity data from the SCAN 97 cruise obtained with the R/V Hespérides and data from the Global Gravity Grid and Sea Floor Topography (GGSFT) database (Sandwell and Smith, 1997) are used to determine the 3D geometry of the crustal-mantle interface (CMI) by numerical inversion methods. Water layer contribution and sedimentary effects were eliminated from the Free Air anomaly to obtain the total anomaly. Sedimentary effects were obtained from the analysis of existing and new SCAN 97 multichannel seismic profiles (MCS). The regional anomaly was obtained after spectral and filtering processes. The smooth 3D geometry of the crustal mantle interface obtained after inversion of the regional anomaly shows an increase in the thickness of the crust towards the continental margins and a NW-SE oriented axis of symmetry coinciding with the position of an older oceanic spreading axis. This interface shows a moderate uplift towards the western part and depicts two main uplifts to the northern and eastern sectors.

KEYWORDS **Gravity. Inverse theory. Antarctic Peninsula. Powell Basin. Marine geophysics.**

INTRODUCTION

The Powell Basin originated during the Cenozoic fragmentation of the NE extremity of the Antarctic Peninsula near the boundary between the Antarctic and South American plates (Fig. 1). This basin can be described as episutural basin (Bally and Snelson, 1980). The Scotia Sea was also formed by this fragmentation because of the drifting of South America and the northern Antarctic Peninsula and the wide-spreading of the continental fragments that connected the two main continents (Barker et al., 1991; Barker, 1995).

The Powell Basin is a small ocean basin (approximately $5x10^4$ km^2) located within the Antarctic Plate, to the NE of the Antarctica Peninsula, close to the limit of the Scotia Plate to the north (Fig.1B). This small oceanic basin is slightly elongated in a NE-SW direction. The chronology of the major events in the development of this basin and its relationship with the surrounding continental blocks, such as the South Shetland Block and South Orkney Microcontinent (SOM; Fig1B), are relatively well known (Larter and Barker, 1991; Livermore and Woollett, 1993; Lawver et al., 1994; Barker, 1995). Rodríguez-Fernández et al., (1997) and Maldonado et al., (1998) using MCS, gravimetric and magnetic data from Russian, Italian and Spanish cruises studied the development of this basin in the context of the whole surrounding area. More recently, Eagles and Livermore (2002) described an opening history of the Powell basin from the interpretation of linear sea floor magnetic anomalies.

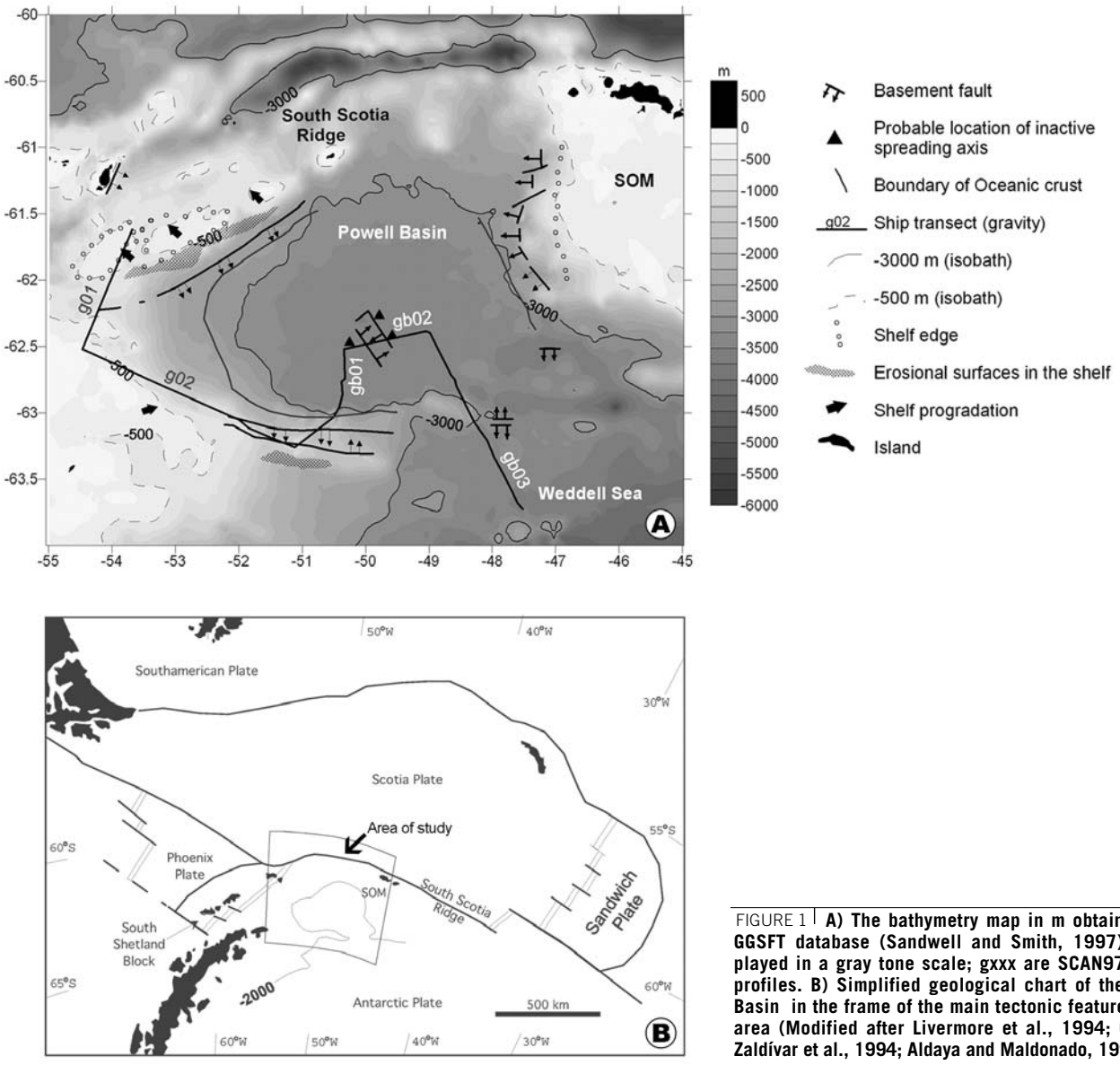

FIGURE 1 **A) The bathymetry map in m obtained from GGSFT database (Sandwell and Smith, 1997) is displayed in a gray tone scale; gxxx are SCAN97 gravity profiles. B) Simplified geological chart of the Powell Basin in the frame of the main tectonic features of the area (Modified after Livermore et al., 1994; Galindo-Zaldívar et al., 1994; Aldaya and Maldonado, 1996).**

The basin bottom is practically horizontal reaching an average depth of 3,200 m, and slightly deepening to the SE (Fig. 1A). The platforms surrounding the basin possess an average depth of 500 m. The northern margins are very steep, whereas the eastern and western margins have gentle slopes. An inactive spreading ridge has been identified located towards the center of the basin with a NW-SE direction. Evidence of this was found from seismic studies carried out in this area (King et al., 1997; Rodríguez-Fernández et al., 1997).

A survey of multichannel seismic profiles (MCS) was carried out during the HESANT 92/93 and SCAN97 cruises with the R/V Hespérides. In addition, gravity data were acquired in the latter cruise. The existing MCS profiles in the area (Coren et al., 1997; Rodríguez-Fernández et al., 1997; Howe et al., 1998; Viseras and Maldonado, 1999) and that obtained in SCAN97 cruise allowed a detailed analysis of the Powell Basin to obtain the structure and the depositional sequences of the continental margins as a whole.

The aim of this study is to determine the 3D crust-mantle interface (CMI) in the oceanic crust of the Powell Basin, by applying numerical inversion of the gravity data. The Global Gravity Data and the Sea Floor Topography databases (Sandwell and Smith, 1997) were employed in combination with the gravity data collected from the ship transects carried out during the SCAN 97 cruise. Thickness of the depositional sequences obtained from detailed study of the available MCS profiles were also used to correct the Free Air gravity data.

REGIONAL TECTONICS

Important crustal fragmentation processes have occurred since the Paleogene in the study area, leading to the rifting and separation of the Antarctic Peninsula from South America. This evolution produced a changing scenario of oceanic plates and continental blocks bounded by transcurrent faults, trenches and spreading ridges (Barker and Burrell, 1977; Henriet et al., 1992; Fig. 1B). The Antarctic, South American and Scotia plates are the main present-day plates in the study area. Moreover, several independent major tectonic elements which were deformed during the complex process of fragmentation of the northern Antarctic Peninsula are also present (Fig. 1B). Most of these elements are now dispersed along the boundaries between the main plates (Barker et al., 1991; Livermore et al., 1993).

The magnetic anomalies of the Scotia Sea recorded the history of the opening of the Drake Passage and the fragmentation and dispersal of crustal blocks around the Scotia Arc, which began more than 29 Ma ago (Barker et al., 1991). This sea contains two plates, the small Sandwich Plate located in the eastern part, which thrusts over the South America Plate, and the larger Scotia Plate separated by a N-S trending ridge (Barker and Hill, 1981; Barker, 1995). Prior to 7 Ma, the Scotia Plate was restricted to the western sector, with a NE-SW trending spreading ridge. Currently, the northern and southern boundaries of both two plates are sinistral transcurrent faults, where the relative motion of South American and Antarctic plates to the W of 25° is accommodated (Barker and Lawver, 1988; Livermore et al., 1993).

The South Shetland block located between the Bransfield Strait and the South Shetland trench, represents the portion of the Antarctic plate thrusting over the extinct Phoenix plate (Maldonado et al., 1993; Aldaya and Maldonado, 1996). The Phoenix Plate has been incorporated into the Antarctic Plate since the cessations of the spreading process at the Phoenix Antarctic ridge at about 3.3 to 5.5 Ma (Larter and Barker, 1991; Livermore et al., 2000). The Shetland Trench is the last remnant of the larger Pacific active margin of the Antarctic Peninsula which was active during the Mesozoic and Cenozoic (Herron and Tucholke, 1976; Larter and Barker, 1991; Maldonado et al., 1994). The South Shetland block extends eastwards into the South Scotia Ridge (Aldaya and Maldonado, 1996). This ridge separates the oceanic domains of the Powell Basin and the Scotia Sea and forms a structural relief composed of grabens and horsts of continental fragments bounded by strike-slip and transtensional faults (Dalziel, 1984; Maldonado et al., 1993; Galindo-Zaldívar et al., 1994). The South Orkney Microcontinent (SOM in Fig. 1), located towards the northeastern end of the study area, is the most important fragment of continental crust in the South Scotia Ridge (King and Barker, 1988), and is considered to be a fragment of the Antarctic Peninsula. It drifted eastwards probably in Late Eocene-Oligocene times, giving rise to the formation of the Powell Basin (King and Barker, 1988; King et al., 1997).

The outcropping formations indicate that mainly low-grade metamorphic rocks make up the upper part of the continental crust. The formation age is comprised between the Paleozoic and the Cretaceous ages (Scotia Metamorphic Complex: Greywacke-shale and Miers Bluff formations, Trinity Peninsula and LeMay groups; B.A.S., 1985). Bodies of basic igneous rocks of Cretaceous age intruded into these formations.

GEOLOGICAL SETTING OF THE POWELL BASIN

The Powell Basin has an almost horizontal basin plain, slightly depressed towards the center and southeast-

ern sectors. The northwestern and southern margins are sharp, rectilinear, and have steep slopes, while the E and W slopes are curved and gentler (Fig. 1A). The Free-Air (FA) gravity anomaly map (Sandwell and Smith, 1997) shows anomalies that correspond well to the main geological features of the basin indicating the location of oceanic crust areas and of continental margins. The Powell Basin is surrounded by continental crustal blocks, except in the south-eastern sector where it is connected with the Jane Basin and Weddell Sea. Coren et al. (1997) have interpreted the southwestern portion of the Powell Basin as an extended continental crust rather than true oceanic crust. In the basin, an irregular arched spreading axis trending NW-SE is deduced from FA gravity anomaly and also revealed by MCS profiles (Coren et al., 1997; King et al., 1997; Maldonado et al., 1998). King et al. (1997) confirmed it as an extinct buried spreading centre. The ridge axis, defined by the gravity low, is linear. It presents a small discontinuity to the south where the width of the basin is much reduced.

Large-amplitude magnetic anomalies (up to 1,000 nT) were found along the HESANT 92/93 profiles in the southern part of the South Scotia Ridge, the northeastern end of the Antarctic Peninsula, and the western end of the continental crust of the SOM. No high-amplitude magnetic anomalies were found in other parts of the surveyed profiles. These large-amplitude magnetic anomalies have been associated to anomalous bodies in the continental basement (Suriñach et al., 1997). These bodies may represent basic igneous rocks, probably gabbros of Cretaceous age, located along the Pacific margin in the Antarctic Peninsula (Garrett, 1990; Maslanyj et al., 1991). Most authors consider this anomaly to be caused by a linear batholithic complex following the arcuate shape of the Antarctic Peninsula. This batholith was probably intruded during crustal extensional episodes of the arc in the active margin (Garrett, 1990). The heterogeneous nature of the continental crust around the basin is evidenced by the analysis of the aero-magnetic data (Ghidella et al., 2002) and Free Air anomalies (Sandwell and Smith, 1997). The magnetic anomalies in the basin plain are of very low amplitude. However, Eagles and Livermore (2002) computed a new magnetic anomaly grid using aeromagnetic and ship data and obtained a pattern of the linear magnetic anomalies trending N30ºW. They produced a model describing a two-stage rift-spreading evolution of the Powell Basin. They found a symmetrical opening with slow spreading rates (16.5-8 km/Ma) and suggesting a spreading age ranging between 29.7 Ma and 21.8 Ma.

Samples dredged from the margins of the Powell Basin consisted of two types of igneous rocks: calc-alkaline and alkaline basalts (Barber et al., 1991). The calc-alkaline rocks of Late Cretaceous age are probably related to the old subduction zones in the Pacific margin of the Antarctic Peninsula between the Antarctic and South American plates. The alkaline basalts are Pliocene to recent in age and were mainly sampled in the northern and southern margins of the basin. Eocene alkaline basalts have also been dredged in the southern margin of the Powell Basin and probably related to the initial stages of the basin opening (Barber et al., 1991).

GRAVITY AND TOPOGRAPHY DATA ANALYSIS

A region of 10° Longitude and 4° Latitude covering the Powell basin was selected. This area is approximately square (45º to 55º W and 60º to 64º S) for this latitude (Fig. 1A). Gravity and bathimetry data were obtained from the version V9.2 of the Global Gravity Grid and the Global Sea Floor Topography database (GGSFT) from http://topex.ucsd.edu (Sandwell and Smith, 1997). Data collected from ship transects corresponding to 5 profiles carried out by the Hespérides, during the SCAN 97 cruise, were also included (Figs. 1A and 2). Gravity data were acquired continuously with a Bell Aerospace Textron BGM-3 marine gravimeter. Data were recorded every 10 s, averaging lectures every 3 min.

The GGSFT database is the latest version of the corresponding prediction inferred gravity and sea-bottom topography from satellite altimeter and shipboard data. Smith and Sandwell (1994) improved the first version to predict bathymetry in the 15-160 km wavelength band. Since 1994, an attempt has been made to improve the wavelength resolution of the predicted bathymetry map. Sandwell and Smith (1997) combined the declassified GEOSAT data (June 1995), the ERS1/2 and Topex/Poseidon data altimeters and a coverage of depth measurements from ship profiles obtained during the last 30 years (See README.15.1 file in http://topex.ucsd.edu/pub). This bathymetric prediction provided the first detailed view of all ocean basins at a 12 km resolution. They obtained the bathymetry, and incorporated the ship depth measurements to constrain the inversion process (Nettleton's Method, Smith and Sandwell, 1994; Sandwell and Smith, 1996).

A detailed description of the limitations on the use of the satellite gravity data is reported in Yale et al. (1998). They pointed out that the level of filtering used in the processing determines the wavelength resolution. We use the V9.1 gravity data version, which is an improved version of version V7.2 (Sandwell and Smith, 1997) with a higher resolution (low pass cut-off wavelength of 14.4 km, see the README.15.1 file. An evaluation of the gravity grid based on the rms difference (in mGal) depicted a good agreement between the satellite gravity data and three

shipboard gravity profiles (README.15.1 file; Yale and Sandwell, 1999). This gravity file encodes the locations of altimeter measurements, allowing us to establish the extent of actual depth measurements used in the predicted grid (Fig. 2).

We used the measured depths from the GGSFT database and the bathymetric data collected by the SCAN 97 profiles (Fig. 2), to establish a whole image of the sea bottom pattern (Fig. 1A, gray tone scale map). The areas not covered by these data were filled with the predicted bathymetry of the GGSFT database. Previous to the merging process of gravity data of the GGSFT database with the gravity data collected from the SCAN 97 field work (g01, g02, gb01, gb02, gb03; observe profiles location in Fig. 1A and GGSFT database in Fig. 2). A numerical correlation was performed in order to determine the resolution of data in the area. The Free-Air gravity anomalies were compared point to point along the 5 profiles. This correlation is shown in Fig. 3. The computed scatter plot presents a correlation coefficient of 0.95, with a fitted slope of 1.01 ± 0.1, and a shift value of 6.1 ± 0.2 mGal. The results of this analysis show a good agreement between marine and GGSFT database, although the GGSFT gravity data represent a smooth version of the observations obtained in the ship. In consequence, we combined the GGSFT database and the SCAN 97 data, giving double weight to this database in the interpolation process.

Fig. 1A presents the bathymetry and Fig. 4 depicts the Free-Air gravity anomaly (FA) resampled in a regular grid with a $\Delta x = 4$ km and $\Delta y = 3.8$ km space interval. The central portion of the basin depicts positive FA anomalies, with a maximum value of 45 mGal. It depicts a trend of minimum values crossing the basin in strike N30ºW. This feature corresponds to the already mentioned inactive spreading center (King et al., 1997; Rodríguez-Fernández et al., 1997; Eagles and Livermore, 2002). Black triangles depict the probable location of this tectonic feature (Figs. 1A and 4). It should be noted the evidence of quasi-symmetry with respect to the axis crossing in the NW-SE direction on this central portion.

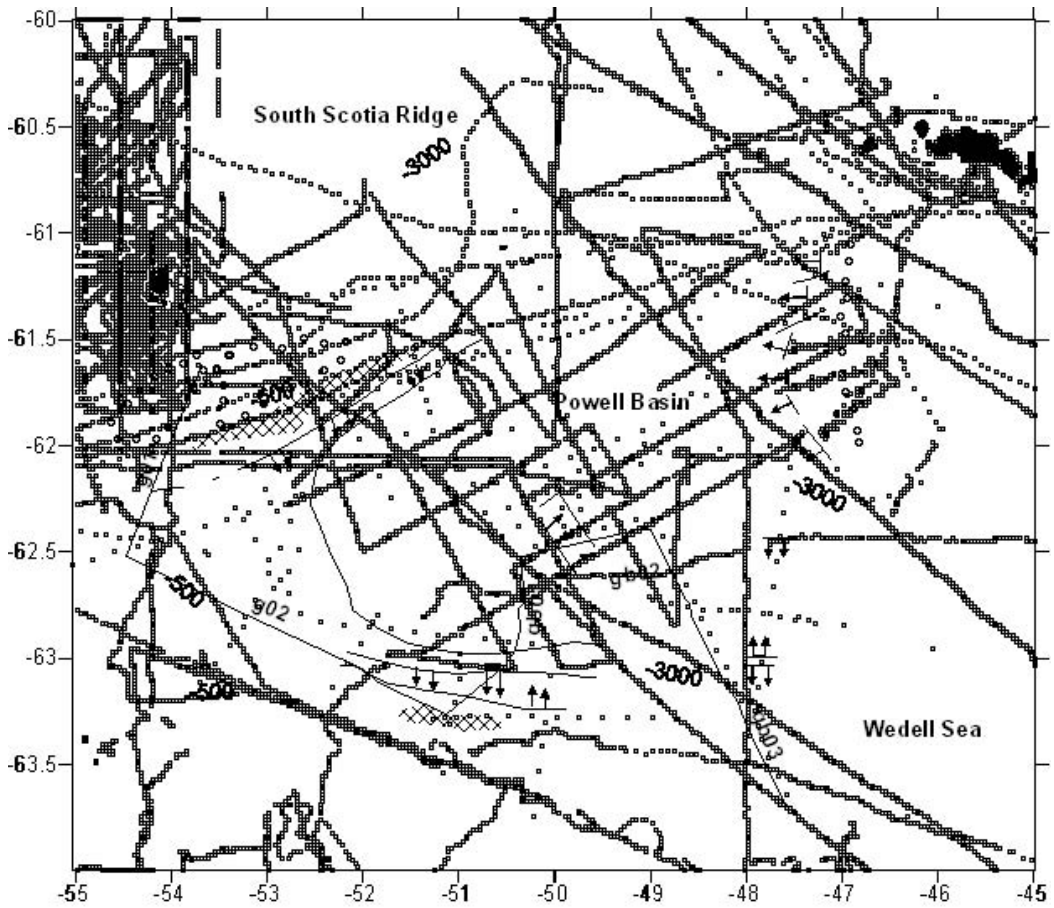

FIGURE 2 | **Location of data employed in this study. Onboard measurements including FA and bathimetry data embedded in the GGSFT database (http://topex.ucsd.edu/cgi-bin/get_data.cgi) are shown as black points. MCS data are displayed as large open squares.**

However, a detailed examination of the Free Air anomaly values depicts higher values to the southern portion of the axis than to the northern region.

Our aim was to use the FA anomaly to obtain the deep crustal structure by employing the inversion method following Suriñach and Chávez (1996), who used it to invert continental Bouguer anomalies. However, the FA anomaly data must be corrected for the layer of water ($g_{w\text{-}s}$) and for the sedimentary thickness ($g_{s\text{-}c}$) gravity effects, which are superimposed onto the FA anomaly (Fig. 4).

The process of correction of the Free Air anomaly involves the stripping (Abdoh et al., 1990) of the gravity contributions of the water and sediments layers and the subsequent incorporation of the gravity contribution of the equivalent volumes assuming the corresponding density values. Therefore, a total gravity anomaly map can be constructed from:

$$\mathbf{gT} = \text{F.A.} - (g_{w\text{-}s} + g_{s\text{-}c}) \quad (1)$$

These two gravity effects are computed by a forward method. Each correction is obtained by computing the gravity contribution produced by a source of infinite lateral extension bounded by a flat surface (z=0) at the top, and a buried or immersed topography at the bottom. These two gravity effects are computed using Parker (1995) algorithm. See Flores-Márquez et al. (2003) for a detailed description of the procedure.

Thus, the FA anomaly data were first reduced by the gravitational attraction of the body of water considering the sea-floor topography (Fig. 1A) obtained from the combined database (GGSFT and SCAN-97) and corrected by the terrain gravity effect. This procedure henceforth will be called water plate correction (Flores-Márquez et al., 2003). The densities employed were estimated from the average velocity model as a function of depth reported by King et al. (1997) by using the relationship reported by Nafe and Drake (i.e. Grant and West, 1965, p. 200) from a considerable number of core samples taken throughout a wide range of depths. These density and velocity models are presented in Fig. 5. Water plate correction was computed using the difference between the mean density of the sediments (2,100 kg/m^3) and the sea water density (1,030 kg/m^3). In consequence, the density contrast used to estimate the water plate contribution is 1,070 kg/m^3. Figure 6A displays this correction, which values range between -140 mGal in the center of the basin and more than 120 mGal over the continental crust.

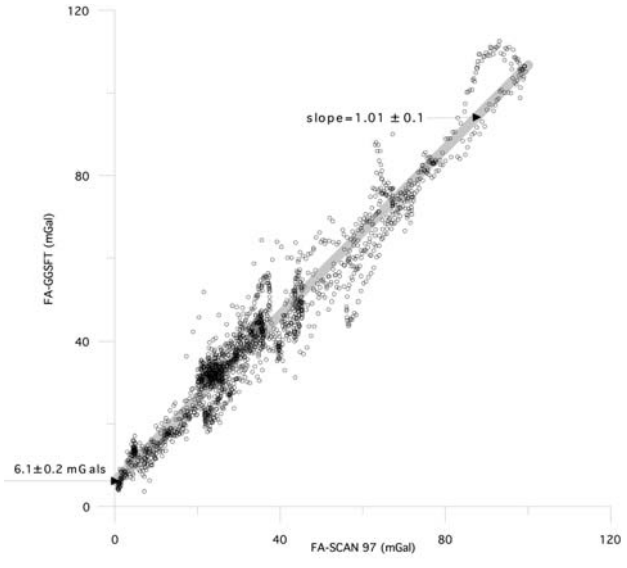

FIGURE 3 | **Correlation between FA data (GGSFT database) and the SCAN 97 project observations.**

Following the same procedure, the gravity effect of the sediments was also calculated. Seismic data from SCAN-97 were incorporated to the existing seismic marine transects (Coren et al., 1997; King et al., 1997; Rodríguez-Fernández et al., 1997) to infer the depth of the sedimentary layer. The bottom morphology of the sedimentary layer was interpolated from these seismic data (open triangles, Fig. 6B) within the Powell Basin area. The recorded depths range between 0.23 km and 5.78 km. A weighted interpolation procedure was employed to estimate the bottom topography of the sediment layer to calculate the corresponding gravity response (Parker, 1995). We have employed the same density for the sediments, whereas the estimated density for the igneous basement (crust) was 2,700 kg/m^3 (Fig.5). A density contrast of 600 kg/m^3 was used to compute the gravity effect of this layer. Figure 6B displays the gravity effect of the sediment layer.

Expression (1) is applied to compute the Total gravity anomaly **gT,** which is shown in Fig. 6C. A conspicuous NW-SE alignment of low gravity values can be observed within the basin in the direction of the inferred location of the inactive spreading axis (black triangles in Fig. 6C). The distribution of the gravity anomalies suggests an asymmetry in the basin, in relation to the axis, being high values to the south-eastern portion. This indicates the presence of a thinner oceanic crust with steep slopes to the NW and a gentle inclination towards the SE. Negative gravity values (dark grey tones) indicating the location of a continental crust bound the Powell Basin, except in the southeastern area (Weddell Sea). To the north, variable positive and negative gravity values (light grey tones) evidence the South Scotia Ridge.

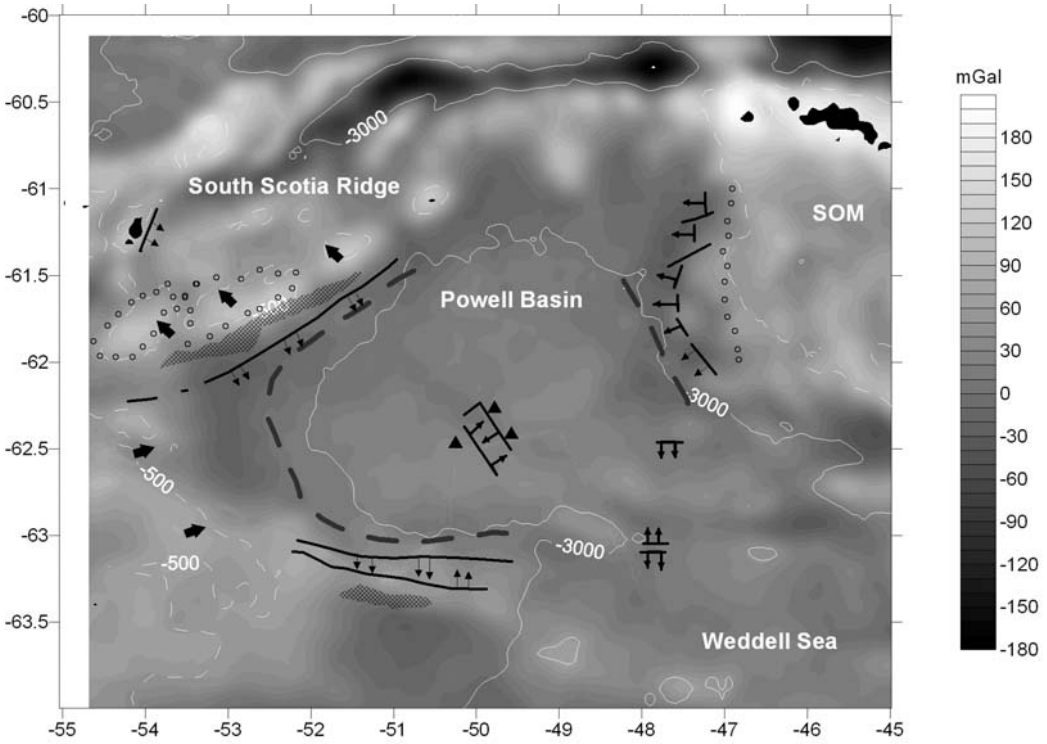

FIGURE 4 | **FA anomaly from combined GGSFT and SCAN 97 databases. Contour interval is 10 mGal. The main tectonic features are overlapped (Figure 1).**

SPECTRAL ANALYSIS

A regional-residual separation process differentiates the main sources composing **gT**. We considered that most of the regional field is due to the variation in the crust-mantle interface (CMI). The Spectral Factorization Method (SFM) (Spector and Grant, 1970) has been applied to estimate the average depth and the cut-off wavenumbers of the different gravity sources composing **gT**. The regional field can be estimated by focusing on the long wavelength sources, which are associated to the CMI. The residual field can also be estimated and related to shallower effects.

The logarithm of the power spectrum of the total gravity anomaly **gT** was analyzed as a function of the radial wavenumbers (Naidu and Mishra, 1972). Figure 7 shows the power spectrum corresponding to the total gravity anomaly. We inferred that the wavenumber K_c= 0.04 km^{-1} separates the domain associated with the regional (low wavenumber content, 0≤K≤0.04 km^{-1}) from the residual (middle wavenumber content, 0.04≤K≤0.08 km^{-1}). This interval may correspond to a boundary located within the crust. King et al., (1997) refer to the existence of two crustal layers (L2 and L3) found in the refraction experiment (Fig. 5, arrow). The ending interval correspond to noisy effects (high wavenumber content, K>0.11 km^{-1}).

Spector and Grant (1970) demonstrated that the slope of the straight line fitted to a selected portion of the spectrum is proportional to the average depth of the gravity

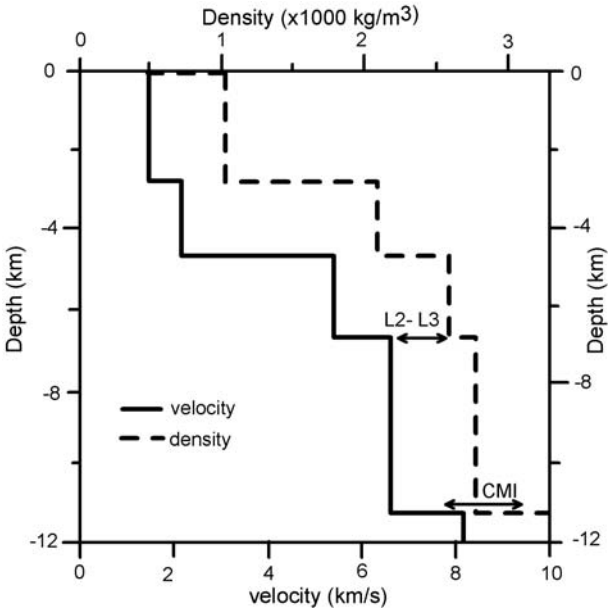

FIGURE 5 | **Velocity-depth structure obtained by King et al. (1997) with the estimated densities via Nafe and Drake's relationship (in Grant and West, 1965, p. 200). Positions of the L2-L3 discontinuity, as well as the CMI are depicted (arrows), as reported by King et al. (1997).**

sources. A linear regression technique was applied to the data within the interval $0<K\leq0.04$ km^{-1} to fit a straight line. An estimated average depth of 14.5 ± 1.1 km was calculated. This result is consistent with a depth of 11.3 ± 2.3 km for the CMI inferred from the refraction study carried out in the northern limits of the Powell Basin (King et al., 1997). The average depth obtained from the power spectrum for the second wavenumber interval

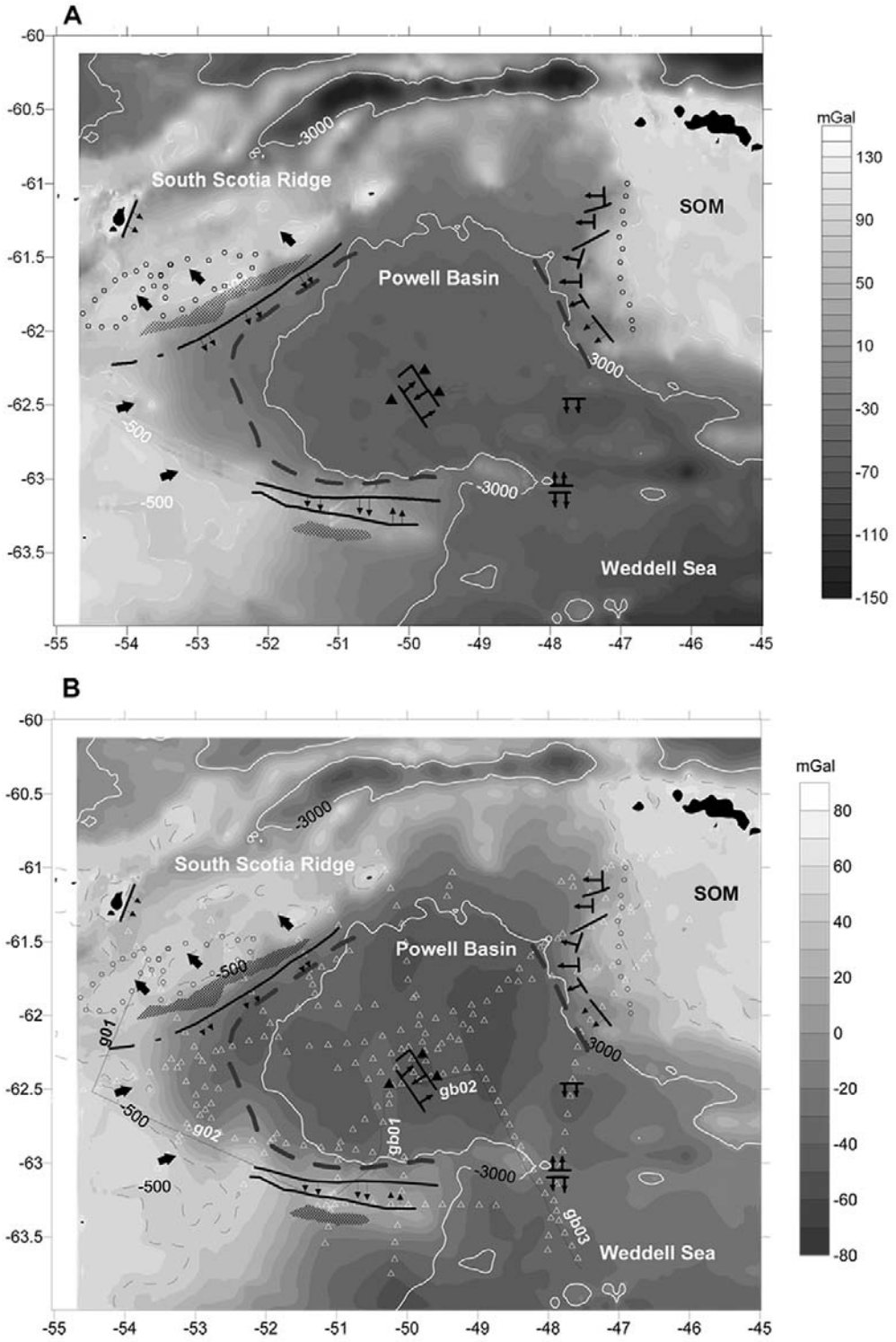

FIGURE 6 | **Gravity contributions for: A) water-sediments interface (controlled by bathymetry from the GGSFT and SCAN97 data (Figures 1 and 2), and B) sediments-basement interface. The geometry of basement was controlled by seismic reflection data (small open triangles). C) The total gravity (gT) anomaly obtained by subtracting (A) and (B) out from the FA anomaly (in Figure 4). Main tectonic features are sown as in Figure 1.**

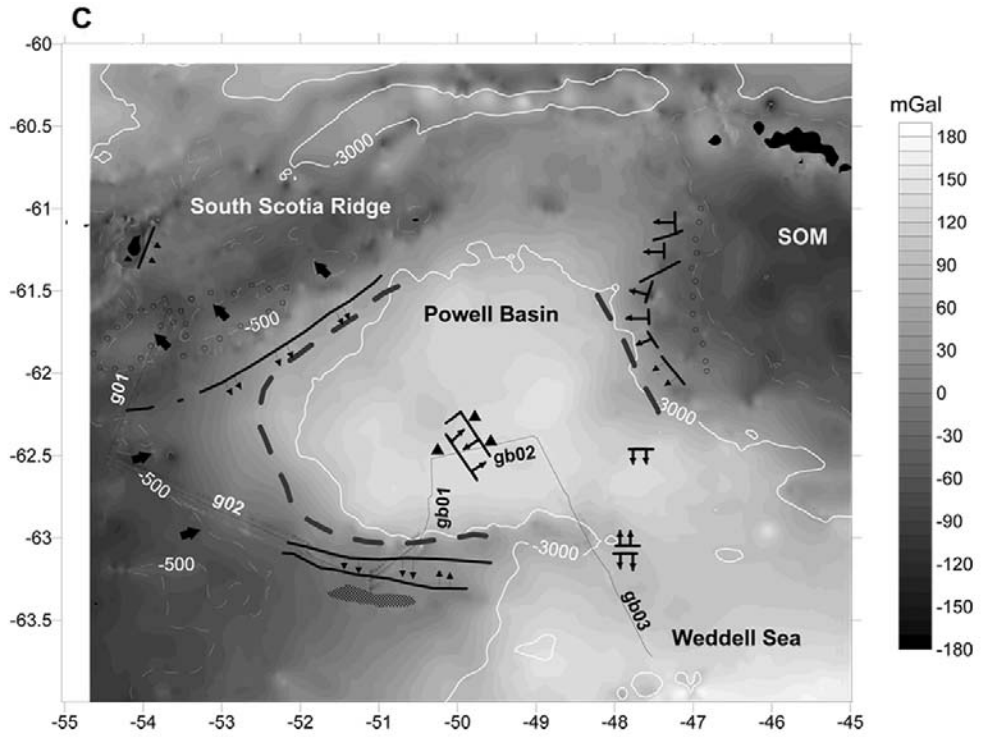

FIGURE 6 | **(Continued)**

(0.04≤K≤0.08 km^{-1}) was 6.9 ± 0.1 km; coincident with the discontinuity L2-L3 in the crust referred by King et al.,1997 (Fig. 5). Nevertheless, it is out of the purpose of this paper to analyze this discontinuity.

A Butterworth filter was designed to isolate the regional field from the total gravity **gT,** with a cut-off wavenumber value of 0.04 km^{-1} and a roll-off term of 0.01 km^{-1}**.** This filtering process was carried out in the wavenumber domain via the Fourier Transform (Gupta and Ramani, 1980; Suriñach and Chávez, 1996). Figure 8 displays the regional field obtained after applying the mathematical filter to **gT**. The field ranges from -56 mGal to 180 mGal and the general trends observed in Fig. 6C are maintained. The central portion of the basin depicts values greater than 130 mGal suggesting a crustal thinning. The inactive spreading ridge is represented as a local gravity low running in the NW-SE direction (Fig. 8). This local gravity low is smaller than that observed in the FA anomaly map. The anomaly values to the NE of the inactive spreading ridge are slightly higher than to the SW.

GRAVITY INVERSION AND RESULTS

We inverted the regional gravity data following Pilkington and Crossley (1986) in order to obtain the CMI topography. These authors extended the two-dimensional inversion method proposed by Oldenburg (1974) to a 3D-inversion procedure. This theory was originally developed to invert gravity data from sedimentary continental basins. Subsequently, the same principle has been applied to model the continental crust (Suriñach and Chávez, 1996) and impact zones (Flores-Márquez et al., 1999). Recently Flores-Márquez et al. (2003) used this methodology to obtain a deep crustal structure of the central Drake Passage (Antarctica).

The inversion method used assumes a model consisting of a single layer over a medium. The boundaries of this layer are a horizontal plane $z=0$ (*upper boundary*), and a surface $z=h(r)$ (*lower boundary*) defining the topography interface (CMI in our case). This surface function is obtained by inverting the gravity data (Fig. 8) over a reference depth $z=z_o$. The irregularities in the interface are considered to be the source of the anomalies. This reference depth is derived from the corresponding spectral analysis of the data (Spector and Grant, 1970). Unsuitable choice of the reference depth, z_o, will produce instabilities in the short-wavelength features of the buried topography (Chávez and Garland, 1985). The final buried topography $h(r)$ is obtained by an iterative method.

The density contrast between the layer and the medium must be assumed as a constant. In general, alternative geophysical methods or previous in situ studies furnish the value of the density contrast. Although there are no values for densities in this area, the refraction study reported by King et al. (1997) may shed some light on the possible densities the crustal rocks and mantle may have. According to Fig. 5, the density of the crust range between 2,700 kg/m^3 and 2,790 kg/m^3, and for the mantle, the density value is 3,300 kg/m^3, approximately. The density contrast varies between 500 kg/m^3 and 600 kg/m^3. The reference depth, z_o, used ranges from 11.5 km following King et al. (1997) to 14.5 km as obtained in this work from the SFM.

A number of inversion trials were performed, varying the reference depth and the density contrast. Chávez and Garland (1985) determined a relation between the density contrast and the depth of reference in terms of the misfit between the computed and observed data. Following these authors, different inversions were carried on for different depths of reference (13 km, 13.5 km, 14 km, and 14.5 km). We found that a depth of 13.5 km minimizes that misfit. The same procedure was done with the density contrast. Four different values for the density contrast were tried (400 kg/m^3, 500 kg/m^3, 600 kg/m^3 and 700 kg/m^3). As Chávez and Garland (1985) reported, we

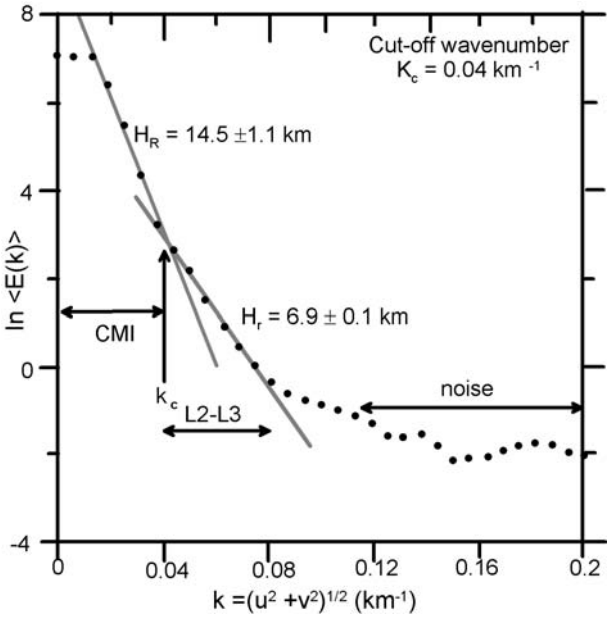

FIGURE 7 | **Averaged power spectrum of gT anomaly (Figure 6C) as a function of the radial wave numbers K. Cut-off wavenumber (K_c) indicates a bound in the spectrum, corresponding to the Crust-Mantle Interface (CMI) effect, with an estimated mean depth of 14.5±1.1 km. The wavenumber interval 0.04≤K≤0.08 km^{-1} depicts the effect of the L2-L3 discontinuity, as reported by (King et al., 1997) to an average depth of 6.9±0.1 km (see Figure 5).**

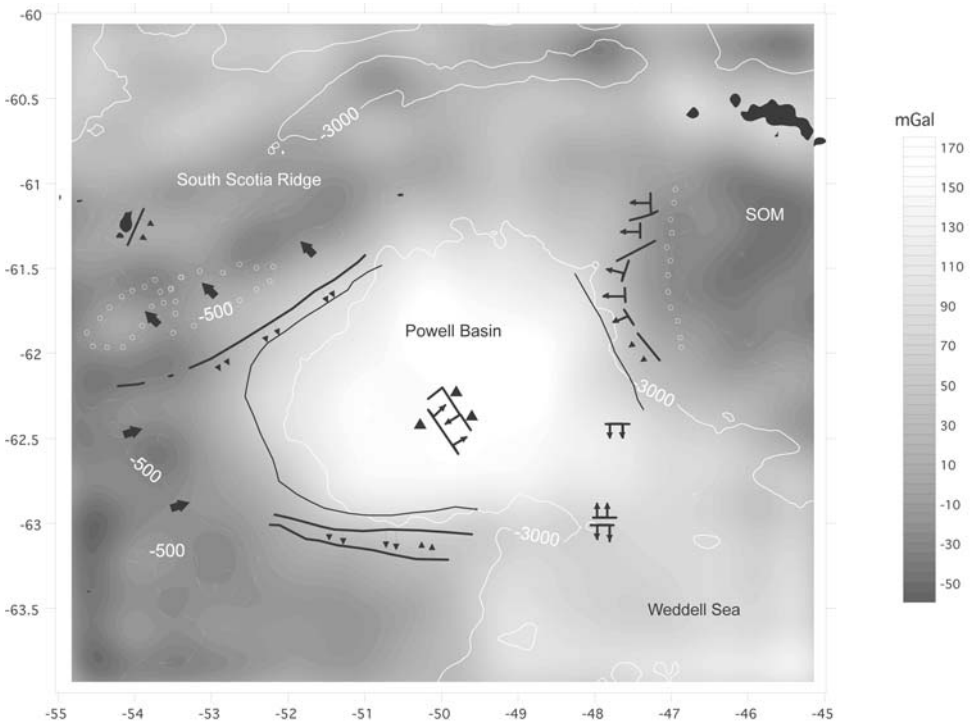

FIGURE 8 | **Regional anomaly field. The low-pass filter applied to Figure 6C was obtained by using the cut-off wavenumber range indicated in Figure 7. Main tectonic features are sown as in Figure 1.**

found that increasing the density contrast, the misfit decreases. On the other hand, lower density contrasts lead to more unreasonable CMI geometries. Combining both approaches, we found that the more reasonable values for the depth of reference z_o and for the density contrast are 13.5 km and 500 kg/m^3, respectively. These parameters are not very far from those estimated for King et al. (1997) for an edge of the basin.

Figure 9 shows the solution (CMI) obtained after four iterations, which minimized the root mean square (rms=0.45 mGal) after using the values mentioned before. The inverted CMI depicts a conspicuous axis, with deeper CMI values trending N30ºW, which coincides with the inactive spreading ridge determined by the MCS profiles (black triangles, Fig. 1A), already discussed by King et al., 1997; Coren et al., 1997; Rodríguez-Fernández et al., 1997 and Eagles and Livermore, 2002. However, as observed in the regional anomaly map (Fig. 8), the extension of this axis is shorter than that depicted in the FA anomaly map (Fig. 4). Depths computed are about 6 km within the central portion of the basin. Depths around 10 km are found in the Weddell Sea area. The computed crustal thickness is in good agreement with the results of the refraction profile reported by King et al. (1997).

The central spreading ridge corresponds to relatively local high CMI depths (1 km difference, approximately) observed within the central portion of the basin, confirming its inactive character, but dividing the basin into two parts. The northeastern half of the basin is slightly wider and has a thinner crystalline crust than the southwestern half of the basin. The MCS profiles in the basin margins (Rodríguez-Fernández et al., 1997) and the asymmetric slopes of the steep starved northeastern and smooth nourished southwestern margins pointed out that the development of the Powell Basin was probably asymmetric and related to a major low-angle normal fault dipping towards the NE. This asymmetric origin of the margins may have determined from the first rifting stages a higher thinning in the eastern part of the basin, which may have follow in some extent during the oceanic spreading. A possible consequence of this process may be faster spreading rates in the eastern half of the basin that developed a thinner oceanic crust than in the western part, although this is not observed in the reconstruction of Eagles and Livermore (2002), probably because their model is based on very weak magnetic anomalies and, indeed, different models may be possible. If we consider, according to Coren et al. (1997), part of the SW sector of Powell Basin of intermediate nature, then, the asymmetry of the basin will be even most marked than that described in this paper.

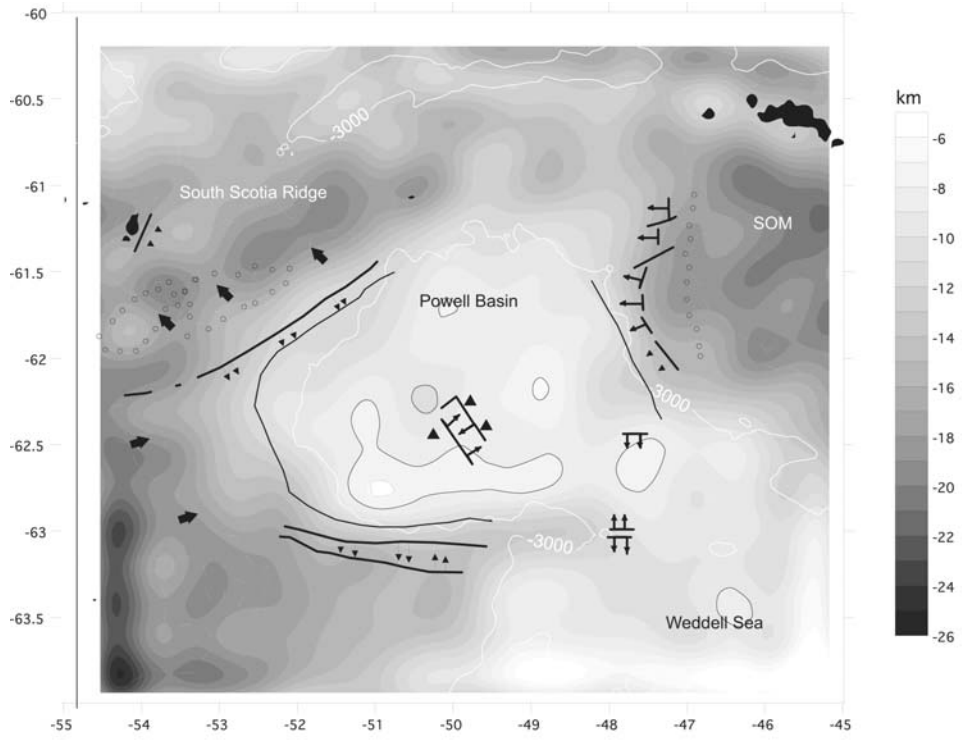

FIGURE 9 | **3D geometry of the CMI. Model is obtained by inversion of the regional anomaly data (Figure 8).**

CONCLUSIONS

Bathymetry and gravity from the combined database (GGSFT and SCAN 97) were used to obtain the CMI of the Powell Basin. Previously, the bathymetry and sediment contributions to the gravity data were eliminated. Sediment correction was obtained from the analysis of the existing MCS profiles. From the spectral analysis the wavenumber interval corresponding to the regional component was obtained. Moreover, a crustal discontinuity situated at 6.9 ± 0.1 km depth was obtained from the spectral analysis, corresponding to that defined by King et al. (1997) from a refraction profile in a northern edge of the Powell Basin. Mean depth of the crustal mantle interface in the Powell Basin was estimated in 13.5 km. The 3D model computed for the CMI yields evidence of a NW-SE oriented axis with relatively deeper values of the CMI, which is coincident with the inferred inactive spreading ridges (King et al., 1997; Rodríguez-Fernández et al., 1997). However, this feature is shorter than that inferred in the FA anomaly map. This fact coincides with the anomaly map obtained by Eagles and Livermoore (2002). A crustal thinning from the continental margins towards the center of the basin is observed. The northeastern part of the basin shows shallower values of the CMI than the western part of the basin. This may be a consequence of the asymmetric origin of the basin, whose rifting is probably related to a low-angle normal fault dipping towards the NE, and during spreading, this asymmetry may have continued in some extent developing a wider north-eastern part of the basin. In addition, the later development of the Jane Basin, connected to the SE of the Powell Basin, may have contributed to increase the asymmetry in between the eastern and western parts.

However, it should be noted, that the inverse process applied produces a single interface with a constant density contrast. In the present paper, lateral variations in density contrast within the crust cannot be modeled. In our opinion, this limitation does not affect our purposes of modeling the oceanic sectors of the Powell Basin CMI because of the smooth trend of the regional gravity anomalies in the area considered.

ACKNOWLEDGEMENTS

We are thankful to the Hespérides Working Group who provided some original data. CGL2004-05646/ANT and University of Barcelona and DGIA-UNAM Interchange program financed this study. The CONACyT, Mexico, also supported Dr. E. L. Flores-Márquez and R.E. Chávez stays at the Universidad de Barcelona.

REFERENCES

Abdoh, A., Cowan, D., Pilkington, M., 1990. 3D gravity inversion of the Cheshire Basin. Geophysical Prospecting, 38, 999-1011.

Aldaya, F., Maldonado, A., 1996. Tectonics of the triple junction at the southern end of the Shackleton Fracture Zone (Antarctic Peninsula). Geo-Marine Letters, 16, 279-286.

Bally, A.W., Snelson, S., 1980. Realm of subsidence: In: Miall, A.D. (ed.). Facts and principles of world petroleum occurrence, Canadian Society of Petroleum Geology, 6, 9-94.

Barber, P.L., Barker, P.F., Pankhurst, R.J., 1991. Dredged rocks from Powell basin and the South Orkney microcontinent. In: Thomson, M.R.A., Crame, J.A., Thompsom, J.W. (eds.). Geological Evolution of Antarctica. Cambridge University Press, 361-367.

Barker, P.F., 1995. Tectonic framework of the Scotia Sea. In: Taylor, B., (ed.). Backarc Basins, Tectonics and Magmatism. Plenum Press, 281-314.

Barker, P.F., Burrell, J., 1977. The opening of Drake Passage. Marine Geology, 25, 15-34.

Barker, P.F., Hill, I.A., 1981. Back-arc extension in the Scotia Sea. Philosophy Transactions of the Royal Society of London A/300, 249-262.

Barker, P.F., Lawver, L.A., 1988. South American –Antarctic plate motion over the past 50 My, and the evolution of the South American -Antarctic Ridge. Geophysical Journal, 94(3), 377-386.

Barker, P.F., Dalziel, I.W.D., Storey, B.C., 1991. Tectonic development of the Scotia Arc region. In: Tingey, R.J. (ed.). Antarctic Geology. Oxford, Oxford University Press, 215-248.

B.A.S., 1985. Tectonic map of the Scotia Arc. Scale 1:300,000, B.A.S.

Chávez, R.E., Garland, G.D., 1985. Linear inversion of gravity data using the spectral expansion method. Geophysics, 50, 820-824.

Coren, F., Ceccone, G., Lodolo, E., Zanolla, C., Zitellini, N., Bonazzi, C., Centonze, J., 1997. Morphology, seismic structure and tectonic development of the Powell Basin: Antarctica. Journal of the Geological Society, 154, 849-862.

Dalziel, I.W.D., 1984. Tectonic evolution of a forearc terrain, Southern Scotia Ridge, Antarctica. Geological Society of America, Special Paper, 200, 32 pp.

Eagles, G., Livermore, R.A., 2002. Opening history of Powell Basin, Antarctic Peninsula. Marine Geology, 185, 195-205.

Flores-Márquez, E.L., Chávez-Segura, R., Campos-Enríquez, O., Pilkington., M., 1999. Preliminary integral 3-D structural model from the Chicxulub impact crater and its implications in the actual geothermal regime. Trends in Heat, Mass and Momentum Transfer, 5, 19-40.

Flores-Márquez, E.L., Suriñach, E., Galindo-Zaldívar, J., Maldonado, A., 2003. 3D Gravity inversion model of the deep crustal structure of the central Drake Passage (Shackleton Fracture Zone and West Scotia Ridge, Antarctica). Journal of Geophysical Research, 108-B9, 2445-2456.

Galindo-Zaldívar, J., Jabaloy, A., Maldonado, A., Sanz de Galdeano, C., 1994. Transtensional deformation and internal basin evolution in the South Scotia Ridge. Terra Antarctica, 1(2) 303-306.

Garret, S.W., 1990. Interpretation of reconnaissance gravity and aeromagnetic surveys of the Antarctic Peninsula. Journal of Geophysical Research, 95/B5, 6759-6777.

Ghidella, M.E., Yáñez, G., LaBrecque, J.L., 2002. Revised tectonic implications for the magnetic anomalies of the western Weddell Sea. Tectonophysics, 347(1-3), 65– 86.

Grant, F.S., West, G.F., 1965. Interpretation Theory in Applied Geophysics. McGraw-Hill, 584 pp.

Gupta, V.K., Ramani, N., 1980. Some aspects of regional residual separation in Precambrian terrain. Geophysics, 45, 1412-1426.

Henriet, P., Meissner, R., Miller, H., Grape Team, 1992. Active margin processes along the Antarctic Peninsula. Tectonophysics, 201, 229-253.

Herron, E.M., Tucholke, B.F., 1976. Sea-floor magnetic patterns and basement structure in the southeastern Pacific. In: Hollister, C.D., Craddock, C.E.A. (eds.). Initial Reports Deep Sea Drilling Project 35, 263-278.

Howe, J.A., Livermore, R.A., Maldonado, A., 1998. Midwave activity and current-controlled sedimentation in Powell Basin, northern Weddell Sea, Antarctica. Marine Geology, 149, 229-241.

King, E.C., Barker, P.F., 1988. The margins of the South Orkney microcontinent. Journal of the Geological Society, 145, 317-331.

King, E.C., Leitchenkov, G., Galindo-Zaldívar, J., Maldonado, A., Lodolo, E., 1997. Crustal structure and sedimentation in Powell Basin. In: Barker, P.F., Cooper, A.K. (ed.). Geology and Seismic Stratigraphy of the Antarctic Margin, Part 2, Antarctic Research Series, American Geophysical Union, 71, 75-93.

Larter, R.D., Barker, P.F., 1991. Effects of ridge crest-trench interaction on Antarctic–Phoenix spreading forces in a young subducting plate. Journal of Geophysical Research, 96, 19586-19607.

Lawver, L.A., Williams, T., Sloan, B., 1994. Seismic stratigraphy and heat flow of Powell Basin. Terra Antarctica 1(2), 309-310.

Livermore, R.A., Woollett, R.W., 1993. Seafloor spreading in the Weddell Sea and Southwest Atlantic since the Late Cretaceous. Earth and Planetary Science Letters, 117, 475-495.

Livermore, R., McAddo, D., Marks, K., 1994. Scotia Sea tectonics from high resolution satellite gravity. Earth and Planetary Science Letters, 123, 255-268.

Livermore, R., Balanya, J.C., Barnolas, A., Galindo-Zaldívar, J., Hernández-Molina, M., Jabaloy, A., Maldonado, A., Martínez, J.M., Rodríguez-Fernández, J., Sanz de Galdeano, C., Somoza, L., Suriñach, E., Viseras, C., 2000. Autopsy on a Dead Spreading Center: The Phoenix Ridge, Drake Passage, Antarctica. Geology, 28-7, 607-610.

Maldonado, A., Aldaya, F., Balanya, J. C., Galindo-Zaldívar, J., Livermore, R. A., Monseñe, F. M., Rodríguez-Fernández, J., Roussanov, M., Sanz de Galdeano, C., Suriñach, E., Viseras, C., 1993. Tectonics and paleoceanography in the northern sector of the Antarctic Peninsula: preliminary results of HESANT 1992/93 cruise with the B/O Hespérides: Sciencia Marina, 57, 79-89.

Maldonado, A., Larter, R., Aldaya, F., 1994. Forearc tectonic evolution of the South Shetland margin, Antarctic Peninsula. Tectonics, 13, 1345-1370.

Maldonado, A., Zitellini, N., Leitchenkov, G., Balanyá, J.C., Coren, F., Galindo-Zaldívar, J., Lodolo, E., Jabaloy, A., Zanolla, C., Rodríguez-Fernández, J., Vinnikovskaya, O., 1998. Small ocean basin development along the Scotia-Antarctica plate boundary and in the northern Weddell Sea. Tectonophysics, 296, 371 - 402.

Maslanyj, M.P., Garret, S.W., Johnson, A.C., Renner, R.G., Smith, A.M., 1991. Aeromagnetic anomaly map of western Antarctica (Weddell Sea sector). Scale 1:2 500,000, B. A. S.

Naidu, P.S., Mishra, D.C., 1972. Radial and angular spectrum in geophysical map analysis: In: Lainiotis, D.G., Tannes, N.S. (eds.). Applications and Information of Control Systems. Reidel Publishing, 447-454.

Oldenburg, D.W., 1974. The inversion and interpretation of gravity anomalies. Geophysics, 39, 526-536.

Parker, R.L., 1995. Improved Fourier terrain correction, Part I. Geophysics, 60, 1007-1017.

Pilkington, M., Crossley, D.J., 1986. Determination of crustal interface topography from potential fields. Geophysics, 51, 1277-1284.

Rodríguez-Fernández, J., Balanya, J.C., Galindo-Zaldívar, J., Maldonado, A., 1997. Tectonic evolution of a restricted ocean basin: the Powell Basin (Northeastern Antarctic Peninsula). Geodinámica Acta, 10(4), 159-174.

Sandwell, D.T., Smith W.H., 1996. Global bathymetric prediction for ocean modeling and marine geophysics. Text in: http://topex.ucsd.edu/marine_topo/text/topo.html.

Sandwell, D.T., Smith, W.H., 1997. Marine Gravity anomaly from Geosat and ERS1 satellite altimetry. Journal of Geophysical Research, 102, 10039-10054.

Smith, W.H., Sandwell D.T., 1994. Bathymetric prediction from dense satellite altimetry and sparse shipboard bathymetry. Journal of Geophysical Research, 99, 21803-21824.

Spector, A., Grant, F.S., 1970. Statistical models for interpreting aeromagnetic data. Geophysics, 35, 293-302.

Suriñach, E., Chávez, R.E., 1996. A 3D crustal model for the northeastern region of the Iberian Peninsula. Geophysical Research Letters, 23, 2457-2460.

Suriñach, E., Galindo-Zaldívar, J., Maldonado, A., Livermore, R.A., 1997. Large amplitude magnetic anomalies in the northern sector of the Powell Basin, NE Antarctica Peninsula. Marine Geophysical Research, 19, 65-80.

Viseras, C., Maldonado, A., 1999. Facies architecture, seismic stratigraphy and development of a high-latitude basin: the Powell Basin (Antarctica). Marine Geology, 157, 69-87.

Yale, M.M., Sandwell D.T., 1999. Stacked global satellite gravity profiles. Geophysics, 64, 1748-1755.

Yale, M.M., Sandwell D.T., Herring A.T., 1998. What are the limitations of satellite altimetry? The leading Edge, 73-76.

Manuscript received November 2005;
revision accepted December 2006.